# Evaluation of Dual Frequency GBAS Performance using Flight Data

Mihaela-Simona Circiu, Michael Felux, Patrick Remi, Lai Yi, Boubeker Belabbas, *German Aerospace Center (DLR)*

Sam Pullen, *Stanford University*

**ABSTRACT**

In this paper, we describe the results of dual frequency Ground Based Augmentation System (GBAS) performance using data from DLR's experimental GBAS testbed and flight trials carried out at the research airport in Braunschweig, Germany. We show the results of noise and multipath evaluation of the new L5 signals from the GPS Block IIF satellites and their application in our experimental GBAS ground station. Results show that, due to the long smoothing time in GBAS processing, there is no clearly visible improvement in terms of $\sigma_{pr\_gnd}$, despite the fact that noise and multipath is significantly lower on the raw (unsmoothed) L5 signals compared to the currently used L1 signals. Two proposed dual-frequency smoothing techniques (Divergence Free and Ionosphere Free) are implemented in the ground and airborne subsystems and tested in comparison with single frequency GBAS performance. During the flight trials, no ionosphere anomaly was observed, thus nominal behavior is presented. In offline analysis, we injected a simulated ionospheric gradient into these raw measurements to compare and evaluate the dual frequency and single frequency techniques and the output of the relevant monitors.

## 1.0 INTRODUCTION

In Safety of Life-critical applications such as civil aviation, high performance requirements in terms of integrity, accuracy, continuity, availability, and robustness against interference need to be achieved. The aim of the Ground Based Augmentation System (GBAS), a development of local-area differential GNSS, is to provide precision approach guidance meeting all of these requirements under low-visibility conditions.

GBAS ground stations supporting CAT I precision approaches (so-called GBAS Approach Service Type C, or GAST-C) are already in service. Standards for CAT III approaches and automatic landings have been defined in the Minimum Operational Performance Standards (MOPS) for GBAS Approach Service Type D [8]. The current GBAS architecture for both GAST C and D is based on the use of GPS satellites and single frequency, L1 C/A code only. Several studies have shown that ionospheric anomalies that cause large spatial gradients pose a significant threat to this system. The use of signals on multiple frequencies and from multiple constellations of GNSS satellites will significantly improve performance compared to the current single frequency (SF) architecture by adding geometric redundancy and allowing ionospheric error estimation and removal. Dual frequency techniques have been investigated in previous work, and two smoothing algorithms, Divergence Free (Dfree) and Ionosphere Free (Ifree) smoothing, have been proposed to mitigate ionosphere gradients [3] [11].

Previous work ([3]) has already reported that semi-codeless measurements from the existing L2 signal (which is not in a protected ARNS band) are much noisier than L5 code measurements. Thus, performance results based on the L1/L2 combination used in this paper are likely to be worse (i.e., more conservative) than for the L1/L5 combination planned for use in the future. However, we found very similar results in terms of noise and multipath performance when analyzing the smoothed B-values of L1, L2 and L5 signals. For this analysis, we used ground receiver measurements of the available L5 signals from the four Block IIF GPS satellites now in orbit. Despite the limited amount of data available from L5 satellites, our results show that, due to the lengthy amount of code-carrier smoothing used in GAST-C GBAS (100 seconds), the difference in terms of ground system performance is surprisingly small between the signals on all three frequencies.

On the airborne side, we analyzed the performance of both Dfree and Ifree smoothing techniques using data from flight trials. DLR conducted several test flights at Braunschweig research airport in November and December 2011 and January 2013. Dual frequency GPS L1 C/A code and semi-codeless L2 measurements were recorded by the receiver onboard the aircraft. Thus, these results are limited to the L1/L2 combination.

During the flight tests, no ionosphere anomalies were observed; thus the first part of the flight trial evaluation section focuses on the performance of Dfree and Ifree smoothing under nominal conditions. In order to investigate potential ionospheric anomalies, an anomalous ionospheric gradient was injected into the raw airborne measurements (using software to modify the stored flight-test values) in the second part of this section. The results

of traditional GBAS single frequency techniques and both Dfree and Ifree dual frequency algorithms are compared. Single frequency (GAST-D) airborne monitor statistics, including code-carrier divergence filtering and dual-solution ionospheric gradient monitoring, are also examined.

## 2.0 TODAY'S GBAS ARHITECTURE

Currently, the fielding of GBAS ground stations supporting CAT-I operations (GAST-C in GBAS terminology) is ongoing. In these systems, the ground station is fully responsible for ensuring the integrity of the signal-in-space component of the position solution which is calculated in the onboard system of each aircraft (in other words, aircraft are only responsible for their own measurement errors). A significant concern for GBAS is the possibility that very large ionospheric gradients could cause a large spatial error decorrelation and thus induce differential position errors for arriving aircraft. One risk mitigation strategy for these errors is to perform "geometry screening" within the ground system by simulating potential errors which could occur under worst-case conditions. If safe error thresholds would be exceeded, the broadcast integrity parameters are inflated to exclude vulnerable satellite geometries from potential use [5].

The same concern about ionosphere-induced error decorrelation exists for GAST-D GBAS systems. The mitigation strategy, however, is a bit different. In this architecture, the ground and airborne systems share the responsibility to ensure no large differential errors can occur without being detected. This is achieved by a combination of several monitors in the aircraft, including the code-carrier divergence (CCD) monitor and the dual solution ionospheric gradient monitor (DSIGMA). Additionally, the airborne subsystem performs its own version of geometry screening and limits the largest impact that one and two potentially affected satellites can have on the estimated position.

With the launch of the Block IIF GPS satellites and the first satellites of the Galileo constellation the broadcast of navigation signals in the L5 band has started. Other than the L2 band L5 is in a protected frequency band and can thus be used for air navigation purposes. The frequency dependent impact of the ionospheric effect brings the possibility of greatly improved detection and mitigation capability in future GBAS architectures which use signals on L1 and L5.

## 3.0 SINGLE AND DUAL FREQUENCY SMOOTHING TECHNIQUES

### Single frequency smoothing

In the current single frequency implementation of GBAS, carrier smoothing is performed to reduce the noise and multipath on code (pseudorange) measurements. This is done by using a low - pass filter as described in Figure 1, where $\rho_1$ is the code measurement and $\phi_1$ is the carrier phase measurement,$\chi$ is the filter input, $\hat{\chi}$ is the output of the filter, and $\hat{\rho}_{smoothed}$represents the smoothed pseudoranges.

In order to remove ranging information from the filter input, the code-carrier difference (code-minus carrier, or CMC) is fed into the low pass filter.Since the ionosphere affects code and carrier measurements by the same amount but with opposite sign, the filter input will contain double the ionospheric delay, as expressed in equation (1).

$$\chi = 2I_1 + \epsilon_1 - N_1 \qquad (1)$$

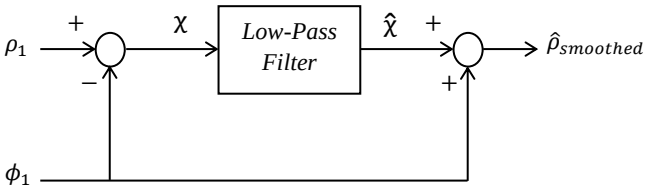


**Figure 1 Low-pass smoothing filter**

After recombining the ranging information by adding the carrier input to the output of the filter, the smoothed single frequency code is expressed by the following (theoretical) equation:

$$\hat{\rho}_{smoothed} = r + \epsilon_{1,smoothed} + (2I_{1,smoothed} - I_1) \quad (2)$$

where $r$ represents the measured geometric range from user to the satellite and $\epsilon_{1,smoothed}$ the smoothed noise on both code and ionospheric error (carrier phase error is neglected, as it is much smaller than the code phase error).

This single frequency filter introduces an additional delay in case the ionosphere varies with time as seen by the user. This effect is called "code-carrier divergence".

### Divergence-free Smoothing (Dfree)

Divergence-free smoothing eliminates ionospheric delay from the filter input and thus removes the code-carrier divergence effect. This is achieved by using a linear combination of dual-frequency carrier phase measurements as the carrier input into the smoothing filter. The expression for the carrier phase input is described in equation (3), where the resulting phase $\phi_{Dfree}$replaces $\phi_1$ as the carrier filter input in Figure 1. The ionospheric delay created by combining the carrier phase measurements has the same sign and magnitude as the one in the code measurements. The code input is the raw code from L1, as in the single frequency case:

$$\phi_{Dfree} = \phi_1 - \frac{2}{\alpha}(\phi_1 - \phi_2) \quad \text{with } \alpha = 1 - f_1^2/f_2^2 \quad (3)$$

$$\rho_{Dfree} = \rho_1 \qquad (4)$$

The smoothed Dfree ranges now do not contain filter-induced divergence, but they still contain the raw code ionosphere error, as can be seen in equation (5).

$$\rho_{Dfree\_smoothed} = r + I_1 + \epsilon_{1,smoothed} \qquad (5)$$

The main advantage of the Dfree solution is that the output noise is similar with to one on the single frequency smoothing, since only one single frequency code measurement is used as the code input (recall that carrier phase noises are small and can be neglected). The impact of an ionospheric gradient, however, can be detected much faster, as is illustrated later in the section about the simulated ionospheric anomaly scenario. The name "Divergence-free" might be misleading sometimes and it refers strictly to a lack of divergence between the filter input and output caused by an ionospheric anomalies.

## 4.0 DLR GROUND FACILITY

DLR has set up a GBAS prototype and algorithm test bed at the Braunschweig research airport (ICAO identifier EDVE), next to the Braunschweig DLR facility.

During the flight trial used for evaluation, the ground system set up consisted of two Javad Delta and one Topcon Net-G3 dual frequency receivers connected to Leica AR 25 choke ring antennas, which were mounted at heights between 2.5 meters and 7.5 meters above the shelters. These receivers were configured to record GPS L1 and (semi-codeless) L2 measurements at a rate of 2 Hz. Recently, the ground station has been updated to include a fourth receiver. In its current configuration, stations BR02, BR03 and BR05 are now using Javad Delta receivers which are capable of tracking L5 and

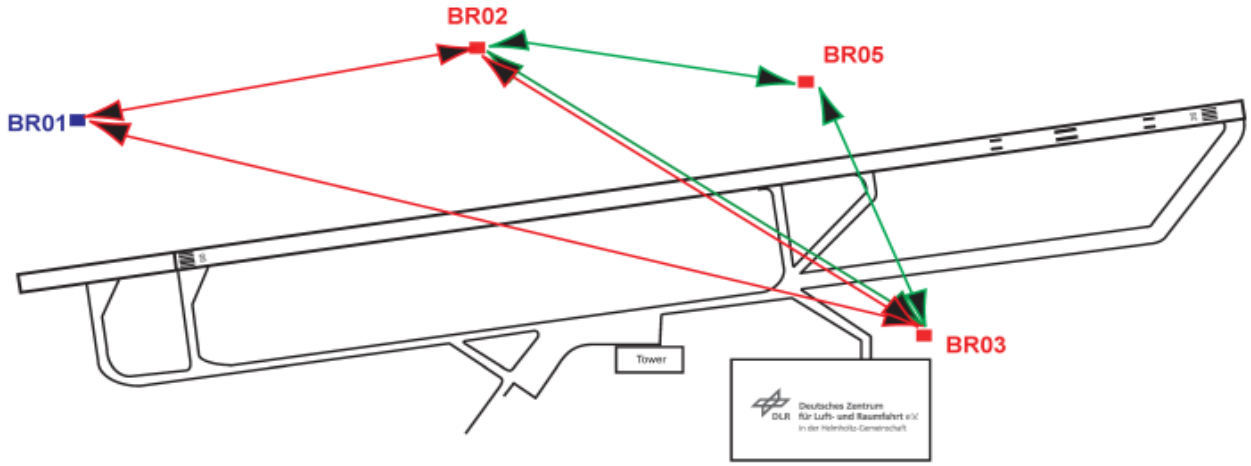


**Figure 2 DLR Ground Facility close to Braunschweig Airport (red – baseline used during the flight, green – baseline for L5 measurements processing)**

**Ionosphere-free Smoothing (Ifree)**

Ionosphere-free smoothing removes ionospheric delay by using ionosphere-free combinations of both code and phase as inputs to the smoothing filter. Both code and phase inputs combine dual frequency measurements, as defined in equations (6) and (7)

$$\phi_{Ifree} = \phi_1 - \frac{1}{\alpha}(\phi_1 - \phi_2) \qquad (6)$$

$$\rho_{Ifree} = \rho_1 - \frac{1}{\alpha}(\rho_1 - \rho_2) \qquad (7)$$

The smoothed Ifree pseudoranges no longer contain ionospheric errors (to a first-order approximation), but they contain the combination of the noise from two code measurements. This increases the noise on the range error and the position solution.

$$\rho_{Ifree\_smoothed} = r + \epsilon_{1,smoothed} - \frac{1}{\alpha}(\epsilon_{1,smoothed} - \epsilon_{2,smoothed}) + \frac{1}{\alpha}(IFB + \tau_{gd}) \qquad (8)$$

Galileo signals in addition to the L1 and L2 capability of the previous receivers.

Figure 2 shows an overview of the current ground station layout, where the red triangle represents the baseline used during the flight trials and the green triangle marks the configuration used for L5 measurement processing.

Even if the guidance for civil aircraft can only be provided by navigation signals that are located within the protected aeronautical frequencies (GPS L1 and L5), an L1 / L2 combination was used with the purpose of testing dual frequency techniques. As the onboard receiver (Topcon Net-G3) is only capable of tracking GPS L1 and L2 signals only those measurements are available for evaluation of the flight trials.

In its previous configuration, the ground station was set up to comply with the GAST-D requirements [14][8], computing and broadcasting corrections and integrity parameters for 30-second and 100-second smoothing techniques. It has been updated to enable application of dual frequency smoothing techniques. This includes

computation of corrections and integrity parameters for 100-second-smoothed Dfree and Ifree pseudoranges as well as calculation and transmission of Dfree and Ifree B-values. 30-second smoothing Dfree and Ifree haven't been considered yet in our processing.

**Ground System characterization**

The B-values represent the integrity parameters associated with the pseudorange corrections provided from each receiver for each satellite, as described in ED - 114A [2] and DO-253C [13]. They are used to detect faulty measurements in the ground system. For each receiver-satellite pair $B(i,j)$, they are computed as:

$$B(i,j) = PRC_{TX}(i) - \frac{1}{M(i)-1}\sum_{k\neq j} PRC_{SCA}(i,k) \qquad (9)$$

where $PRC_{TX}$ represents the candidate transmitted pseudorange correction for the satellite $i$ (computed as an average of all receivers), and $PRC_{SCA}$ represents the correction for satellite $i$ from receiver $k$ after smoothed clock adjustment, which is the process of estimating and removing the individual receiver clock bias from each reference receiver and all other common errors from the corrections. If all B-values are below their thresholds, the candidate pseudorange correction $PRC_{TX}$ is approved and transmitted. If not, a series of measurement exclusions and *PRC* and B-value recalculations takes place until all revised B-values are below threshold.

Under the assumption that multipath errors are uncorrelated across reference receivers, nominal B values can be used used to assess the accuracy of the ground system. The standard deviation of the uncertainty associated with the contribution of the corrections ($\sigma_{pr\_gnd}$) is related to the standard deviation of the B values by:

$$\sigma^2_{pr\_gnd} = \sigma^2_B \frac{(M-1)(N+1)}{N} \qquad (10)$$

with N being the number of satellites used (i.e, the number of satellites for which corrections are broadcast) and M being the number of reference receivers used (M = 3 in our case). The standard deviation of the B values is computed by sorting the data into elevation bins with bin sizes of 1° up to a satellite elevation of 30°, 2° between 30° and 50°, and 5° for all higher elevations. In order to provide samples that are approximately independent in time, one B value was considered every $2\tau$ seconds, with $\tau$ being the smoothing time constant used to generate the corrections. More details about the assessment of $\sigma_{pr\_gnd}$ are described in ED-114A [2].

We performed $\sigma_{pr\_gnd}$ evaluation using B-values generated using the single frequency smoothing technique with 30-second and 100-second time constants (both used in GAST-D) as well as with B-values generated using Dfree and Ifree smoothing techniques with a 100-second time constant. The data evaluated was recorded on 17th of January 2013 over 24 hours. Evaluation was performed for each receiver individually, and the broadcast value of $\sigma_{pr\_gnd}$ for each elevation bin is the maximum over all three receivers. Based on the computed $\sigma_{pr\_gnd}$, each ground subsystem is classified into one of the three categories, representing the ground accuracy designators (GAD A, B and C). A detailed description of these accuracy models can be found in [9].

The results of the final broadcast $\sigma_{pr\_gnd}$ using SF 30-second smoothed (orange curve), SF 100-second smoothed (magenta curve), Dfree 100-second smoothed (blue curve), and Ifree 100-second smoothed (black curve) measurements are shown in Figure 3. The dashed lines represent the ground accuracy models.

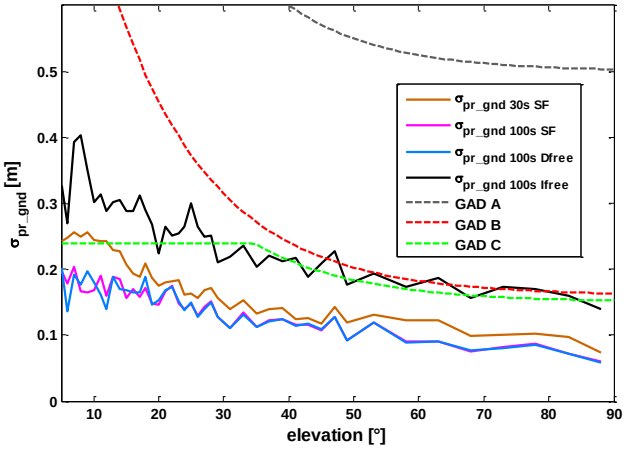


**Figure 3 Evaluated $\sigma_{pr\_gnd}$ for SF 30s (orange), SF 100s (magenta), Dfree 100s (blue), Ifree 100s (black) and GAD curves**

As expected, the single frequency values smoothed with a 100-second time constant are smaller than the ones with a 30-second smoothing constant, but the ratio is below the theoretical value of $\sqrt{100/30} = 1.8$. The theoretical model assumes that the noise is a pure white process, which is not the case using real measurements that contain multipath errors. The ratio we found was in the range of 1.3, which conforms with the results found by Boeing in their studies [10].

Dfree 100-second smoothed values are very similar to the ones obtained with 100-second single frequency smoothing, since they have the same level of noise: both contain multipath and noise from L1 C/A code only. The higher noise on Ifree, obtained from the combination of the two code measurements, leads to a higher value of $\sigma_{pr\_gnd}$. Ifree with 100-second smoothing has errors almost double that of 100-second-smoothed SF and exceeds the green dashed GAD C curve in Figure 3.

As stated earlier, the results shown in Figure 3 are based on L1 and semi-codeless L2 measurement combination. For aviation, the L1/L5 combination is of interest since both signals are located in protected Aeronautical Radio Navigation Service (ARNS) frequency bands. The

difference between L1 C/A and L5C signals are the chipping rate of the ranging code and the signal power. L5 has a chipping rate which is 10 times higher than the L1 chipping rate and has four times higher signal power. This contributes to an improvement in signal acquisition and tracking. Multipath and thermal noise are expected to be smaller on L5 measurements compared with L1 measurements, but it is unclear how much smaller. This was confirmed by our measurements and calculations. In Figure 4, estimates of unsmoothed multipath and noise errors on L1, L2 semi-codeless and L5 are plotted as a function of satellite elevation using measurements from the four available IIF GPS satellites which already provide L5C signals. Multipath and noise are estimated using the linear dual frequency combinations described in equations (11) and (12) [7], where $MP1$ represents the code multipath and noise on the first frequency, $MP2$ represents the code multipath and noise on the second frequency, $\rho_i$ represents code measurements, and $\phi_i$ represents carrier-phase measurements on frequency $i$. The remaining biases are assumed to be constant and are removed by averaging over a fixed number of epochs (i.e., 50 epochs).

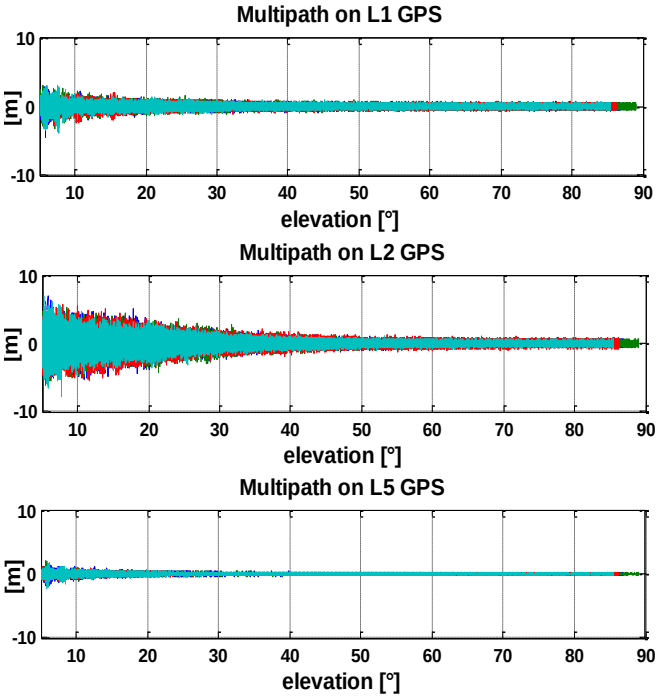


**Figure 4 Raw multipath and noise error versus satellite elevation for L1 C/A code (top plot), L2 semicodeless measurements (middle plot) and L5C (bottom plot)**

$$MP1 = \rho_1 - \left(1 + \frac{2}{\alpha-1}\right)\phi_1 + \left(\frac{2}{\alpha-1}\right)\phi_2 \qquad (11)$$

$$MP2 = \rho_2 - \left(\frac{2\alpha}{\alpha-1}\right)\phi_1 + \left(\frac{2}{\alpha-1} - 1\right)\phi_2 \qquad (12)$$

Higher multipath and noise error on L2 is expected due to the use of semi-codeless tracking. Multipath and noise error on L5 is reduced substantially from L1, with a ratio varying from 2 up to 3 in our evaluations. However, these are preliminary results of L5 measurements, and they are subject to further investigation. To further explain these results, antenna pattern and multipath polarization differences for L1 and L5 have to be taken into account.

In the next step, we have evaluated the $\sigma_{pr\_gnd}$ based on L1, L2 and L5 signals smoothed separately (i.e., using SF) for 100 seconds, and the results are illustrated in Figure 5. Data over five days was collected from the ground reference receivers at Braunschweig, and only the four Block IIF GPS satellites were considered. The amount of data derived from using only these four satellites is much lower than the amount derived from using all GPS satellites that broadcast L1 and L2 signals. This may explain the larger error values compared with the previous values shown for 100-second smoothed L1 $\sigma_{pr\_gnd}$ shown in Figure 3.

The most interesting result, however, is that, despite having the different raw multipath characteristics shown in Figure 4, the values of 100-second smoothed $\sigma_{pr\_gnd}$ on L1, L2 and L5 are very similar in Figure 5. This effect appears to be due to the effect of 100 seconds of smoothing, which attenuates most of the multipath frequencies that differ between L1, L2 and L5 and leaves only those with time correlations larger than 100 seconds that are the very similar.

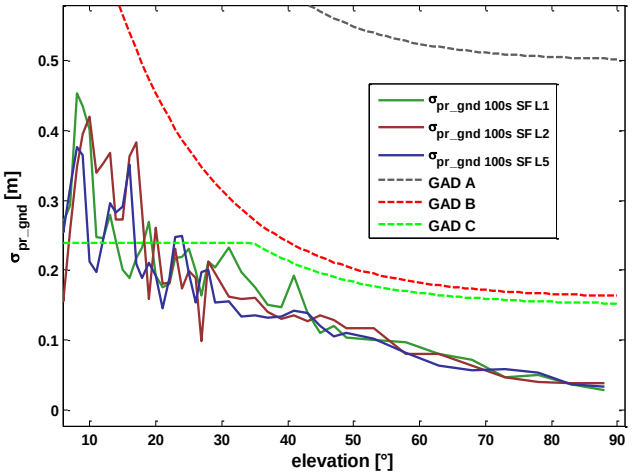


**Figure 5 Resulting $\sigma_{pr\_gnd}$ for L1, L2, and L5 using 100-second smoothing**

To confirm this, we generated unsmoothed B-values for L1, L2 and L5 and smoothed B values using several increasing values of smoothing time constants. In Figure 6 Unsmoothed B values for L1 (top plot), L2 (middle plot), L5 (bottom plot) are shown. As expected, they are very similar to the results in Figure 4. Multipath and noise errors are significantly attenuated by 30 seconds of smoothing, as can be observed in Figure 7, but there are still differences between L1, L2 and L5. This difference shrinks as the smoothing time constants increased.

Smoothing with a time constant of 100 seconds removes the multipath difference almost completely.

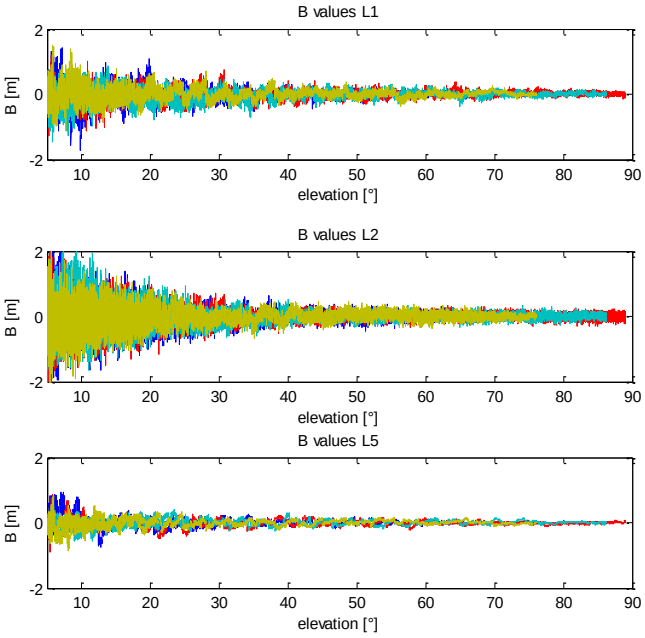


**Figure 6 Unsmoothed B values for L1 (top plot), L2 (middle plot), L5 (bottom plot)**

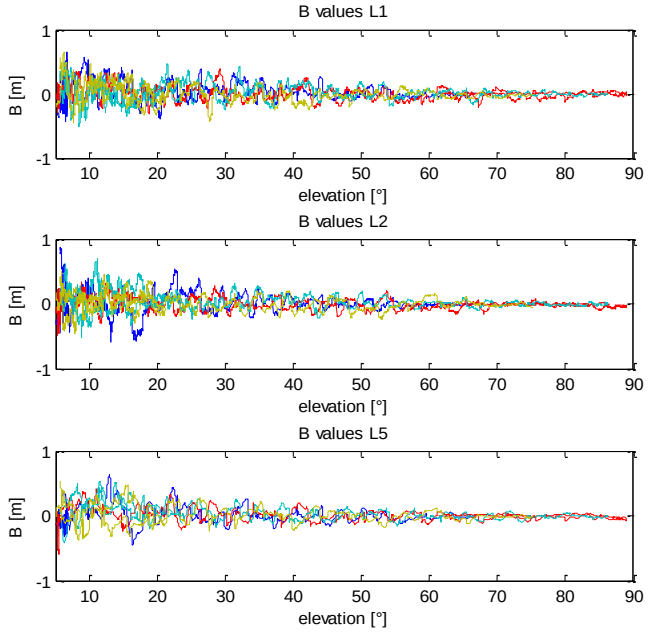


**Figure 7 30-second-smoothed B -values for L1 (top plot), L2 (middle plot) and L5 (bottom plot)**

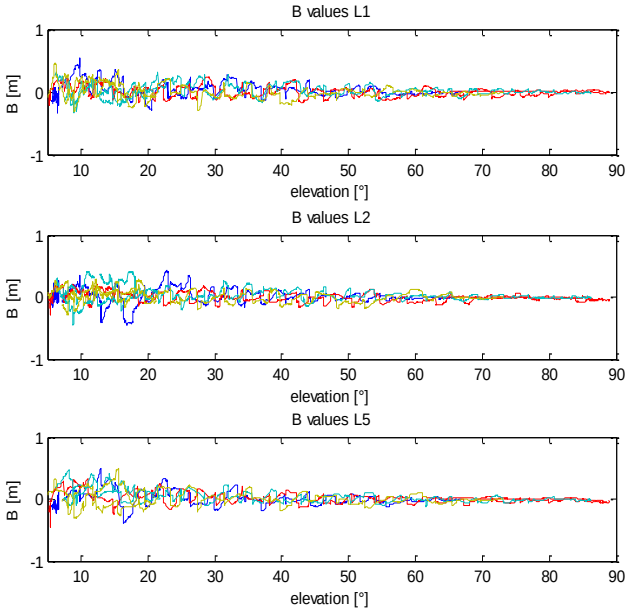


**Figure 8 100-second-smoothed B -values for L1 (top plot), L2 (middle plot) and L5 (bottom plot)**

## 5.0 FLIGHT TRIALS AND DATA PROCESSING

### Flight Trial

The results shown in this section were recorded during a flight trial which took place within the DLR internal project TOPGAL on January 18, 2013. The flight was carried out with DLR's Airbus A320 research aircraft "ATRA," which was equipped with a Topcon Net-G3 GNSS receiver recording GPS measurements on L1 and L2 at a rate of 10 Hz. Figure 9 shows the aircraft and the location of the GNSS antenna.

The purpose of this flight was to evaluate GBAS GAST-D performance in real-time, collect data for further dual-

**Figure 9 DLR's Airbus A320 research aircraft "ATRA". The location of the experimental GNSS antenna is marked by the red arrow**

frequency evaluations, and characterize the loss of satellite signals in turns at different aircraft bank angles.

These maneuvers lead to a significant decrease in performance at a 45° bank angle and a complete loss of GBAS guidance when full circles at a bank angle of 60° were flown. Furthermore, different curved approaches were investigated from an operational point of view. The procedures, pilot interfaces and results from an operational perspective were presented in [12]. The flight examined in the paper and used for iono simulations lasted for 2.5 hours, and a total of six approaches with subsequent go-arounds to Braunschweig's runway 08 and one final landing were conducted. However, due to hardware issues, useable data is only available for the first three approaches and will be presented here. As a truth position reference for performance evaluations, we use a post-processed dual frequency carrier phase position solution obtained from Novatel's GrafNav software in a combined forward-backward smoothing mode. The ground track of the aircraft flight path is shown in Figure 10.

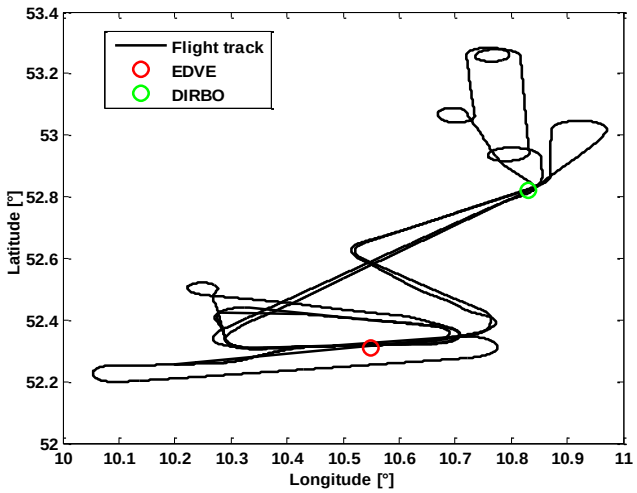


**Figure 10 Ground track of the flight trial (EDVE is the ICAO identifier for Braunschweig airport)**

GBAS has to protect all users during the critical approach phase and ensure system integrity. This is achieved by comparing vertical and lateral protection levels (VPL, LPL) to the respective alert limits (AL). Protection levels are conservative overbounds of the maximum position error after application of the differential corrections provided by the ground system.The alert limits vary with the distance of the aircraft to the landing threshold point and represent tolerable margins for the position error which do not endanger the aircraft. The lateral alert limit decreases from 63.15 m to a value of 40 m on the final approach segment close to the runway threshold. The vertical alert limit decreases from 43.35 m to a value of 10 m on the final approach segment close to the runway threshold. The alert limits are computed as defined in GAST-D RTCA-MOPS [13].

Equations 13 and 14 express the nominal protection levels for GAST-D as detailed in section 2.3.11.5.2.1.4 of the RTCA MOPS [13],

$$VPL = K_{ffmd}\sqrt{\sum_{i=1}^{N} S_{apr,vert,i}^2 \sigma_i^2} + D_v \qquad (13)$$

$$LPL = K_{ffmd}\sqrt{\sum_{i=1}^{N} S_{apr,lat,i}^2 \sigma_i^2} + D_l \qquad (14)$$

$$\sigma_i^2 = \sigma_{pr\_gnd}^2 + \sigma_{air}^2 + \sigma_{iono}^2 + \sigma_{tropo}^2 \qquad (15)$$

where $K_{ffma}$represents the fault free missed detection multiplier, $S_{apr}$ the weighted pseudoinverse of the geometry matrix which translates the measurements from the pseudorange domain into the position domain, and $\sigma_i$ the standard deviation of the uncertainty of the residual differential pseudorange error. $D_v$ and $D_l$ are GAST-D specific terms that represent the magnitude of the vertical and lateral projection of the difference between 30-second and 100-second smoothed positions. Dual frequency protection levels were computed by using equations (13-14) with $D_v = D_l = 0$, since for dual frequency we considered only the solution based on 100-second smoothed solution.

The standard deviation of the residual uncertainty of the differential GBAS error $\sigma_i$ consists of the root-sum-square of uncertainties introduced through ionospheric and tropospheric decorrelation as well as the contribution of the ground and airborne multipath and noise, as defined in equation (15). In order to calculate the protection levels for dual frequency techniques, each individual sigma in equation (15) has to be reevaluated, as they differ for each technique.

The standard deviation associated with the ground contribution ($\sigma_{pr\_gnd}$) was discussed in the previous section. The computed values based on real measurements were broadcast to the airborne system. For single frequency GAST-D, $\sigma_{pr\_gnd}$ used in the protection levels and weighting is obtained from 30-second smoothed data.

Residual airborne receiver noise ($\sigma_{air}$) consists of multipath and thermal noise as expressed in equation (16). For single frequency GBAS, GPS L1 measurements standard models called Airborne Accuracy Designators (AAD) were presented by McGraw et al. in [9] considering different airborne receivers. They proposed two types of designators: AAD A and AAD B. For our case, the more conservative AAD A was used and is defined in equations (17) and (18) (the resulting values are in meters or meters$^2$).

$$\sigma_{air\_SF}^2 = \sigma_{mp}^2 + \sigma_n^2 \qquad (16)$$

$$\sigma_n = 0.15 + 0.43e^{-el/6.9} \qquad (17)$$

$$\sigma_{mp} = 0.13 + 0.53e^{-el/10} \quad (18)$$

However, there are no models defined for dual frequency processing. The noise and multipath level of the Dfree solution is similar to that of single frequency smoothing since both use L1 C/A code measurements as inputs. Thus, the residual airborne noise and multipath on the output of Dfree is considered to be the same as thatfor single frequency.

$$\sigma_{air\_Dfree} = \sigma_{air\_SF} \quad (19)$$

Unlike Dfree, the Ifree technique combines two code measurements which leads to higher noise, as explained earlier in Section 3.0. The ratio between $\sigma_{air\_Ifree}$ and $\sigma_{air}$ was chosen to be the maximum value of the ratio between the $\sigma_{pr\_gnd}$ values for Ifree and single frequency with a 100-second smoothing time constant. This ratio is 2.33 which is below the theoretical value of 2.98 used in [4]. Even if we consider that the standard deviation of residual error for 100-second smoothed L1 code and 100-second smoothed L2 code are roughly the same (as found in our ground evaluation), theoretical model assumes that the noise is a pure white process, which we know is not valid. This helps to explain the difference between the ratio obtained from measurements and the theoretical one. Thus, we used the measured ratio:

$$\sigma_{air\_Ifree} = 2.33\ \sigma_{air\_SF} \quad (20)$$

The standard deviation of residual troposphere error does not change in the dual-frequency case since the troposphere is non-dispersive and does not depend on frequency. The residual error depends on atmospheric conditions and on the difference in altitude between the aircraft and the ground. The model we used for $\sigma_{tropo}$ is the one defined in Section 2.3.12.2 of the RTCA MOPS [13].

The residual ionospheric error after differential correction is different among the three techniques; thus $\sigma_{iono}$ has to be adapted to each case. For single frequency smoothing, $\sigma_{iono}$ is defined in Section 2.3.12.3 of the RTCA-MOPS [13] as:

$$\sigma_{iono} = F_{pp}\sigma_{vig}(x_{air} + 2\tau v_{air}) \quad (21)$$

where $F_{pp}$ is the vertical-to-slant obliquity factor [13], $\sigma_{vig}$ is the standard deviation of nominal ionospheric uncertainty due to special decorrelation, $x_{air}$ is the 2-D horizontal distance between ground station and user, $\tau$ is the smoothing time constant (30 seconds for GAST-D), and $v_{air}$ is the ground speed of the aircraft. The term $2\tau v_{air}$ represents the additional error introduced by single frequency smoothing due to the ionospheric divergence created by an aircraft moving through a spatial ionospheric gradient with horizontal velocity $v_{air}$.

Dfree smoothing corrects for this divergence, but it retains the absolute ionospheric delay difference between ground and air. Considering this, $\sigma_{iono}$ for Dfree is described as:

$$\sigma_{iono\_Dfree} = F_{pp}\sigma_{vig}x_{air} \quad (22)$$

Ifree removes ionospheric delay completely (to first order) at both ground and airborne receivers; so no ionosphere-related errors remain to be considered:

$$\sigma_{iono\_Ifree} = 0 \quad (23)$$

For both single frequency and Dfree, we used a value of 4 mm/km for $\sigma_{vig}$, the conservative value determined for the CONUS region. [6]

Figure 11 shows the results obtained during three approaches from our flight trial. During one of the turns, at minute 20, we had a hardware problem and our receiver did not track any data for a period of 10 seconds. All smoothing filters had to be reinitialized, resulting in a data gap for a period of 6-7 minutes. After recovering, a steep bank angle turn resulted in loss of lock on all but three satellites. For these epochs, the vertical protection levels exceeded the alert limits for all three techniques due to the bad geometry which prevailed after loss of all low-elevation satellites. During the rest of the flight, Dfree and GAST-D protection levels, as well as the respective vertical errors, are very similar to each other as expected. Ifree protection levels and vertical errors are larger, due to the larger noise and multipath error in Ifree smoothing. However, the Ifree vertical protection levels are below the vertical alert limit at all times (except during the unusual maneuvers noted above).

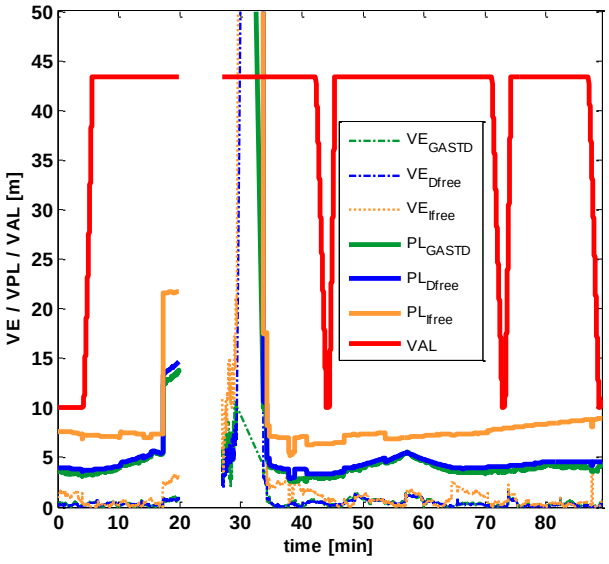


**Figure 11 Calculated VAL (red curve), VPL for GAST-D (green), VPL for Dfree (blue curve), and VPL for Ifree (orange curve). The dashed lines represent actual errors.**

Figure 12 contains three vertical Stanford plots for the GAST-D, Dfree and Ifree solutions, respectively. These plots are divided into four areas: nominal behavior (white area), system unavailable (yellow area), misleading information (orange and light red areas) and hazardously misleading information (red area). Under nominal conditions, the navigation system error (NSE) is smaller than the protection level, which in turn is smaller than the alert limit. The system becomes unavailable when the protection level exceeds the alert limit (a fact which is known to the user). If the navigation system error is larger than the protection level, misleading information is given to the system. Misleading information becomes hazardous to the aircraft if the error exceeds the alert limit. In the plots, both navigation error and protection level axes are normalized by the alert limit at a given time, since the alert limits vary with distance to the runway.

During the flight, the system was unavailable only during one steep bank angle turn, and at no time did misleading information or hazardously misleading information occur. In addition, no GAST-D monitor flagged or alerted during the normal parts of the flight trial.

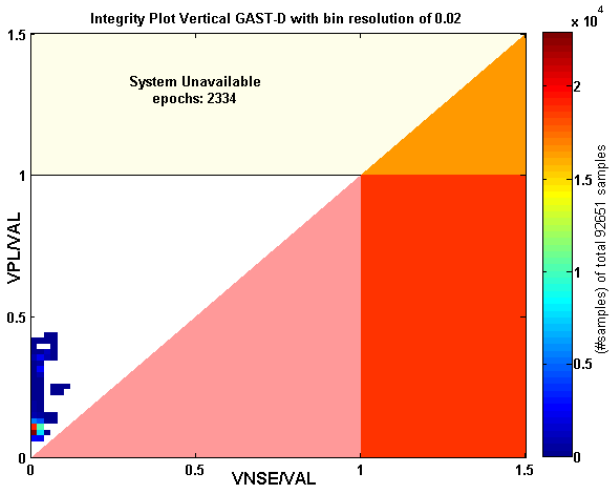


**(a)**

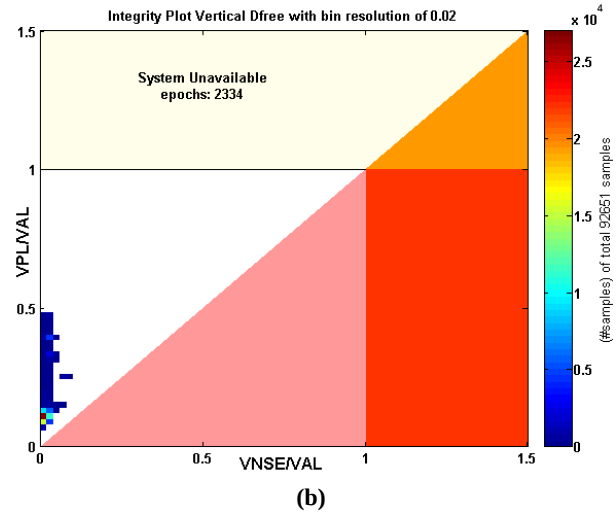


**(b)**

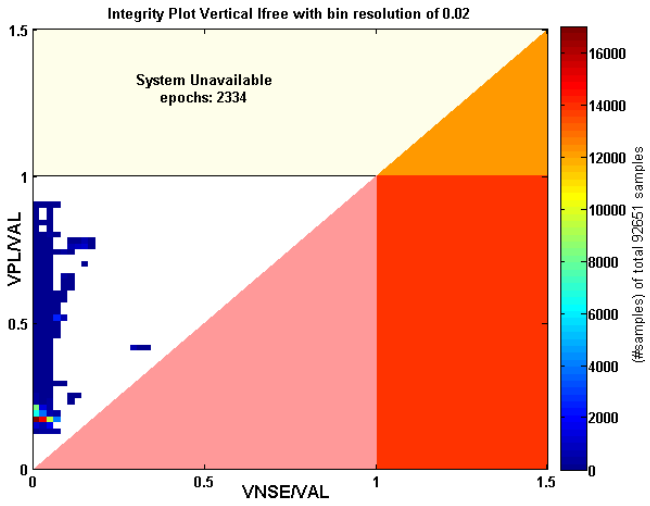


**(c)**

**Figure 12 Integrity assessment using data collected during flight trials for (a) GAST-D, (b) Dfree, (c) Ifree**

## 6.0 IONOSPHERIC ANOMALY

Since the flights were performed on quiet ionospheric days, we injected an anomalous ionospheric gradient into the raw measurements in post-processing. The artificial ionospheric error $\delta iono_{injected}$ as a function of time $t$ since the onset of the gradient is defined in equation (24). The gradient is inserted only on the airborne measurements, meaning that the ground is not affected by this gradient during the run-time of this offline simulation.

$$\delta iono_{injected}(t) = \alpha \Delta\tau t V_{front} \ [m] \qquad (24)$$

where:

$\alpha \quad = gradient\ size\ [mm/km]$

$\Delta\tau \quad = sampling\ interval\ [s]$ (0.05s for our case)

$V_{front} \ = relative\ front\ speed\ [m/s]$

One goal of this study is to examine the behavior of each smoothing technique under anomalous ionospheric scenarios. Recall that the ionosphere impacts code and carrier phase measurements differently. It induces a delay into the code and an equal-but-opposite "advance" into the phase measurements. Taking this into consideration, the same bias with opposite sign is applied to the L1 measurements as shown in equations (25) and (26).

$$\rho = \rho_{raw} + \delta iono_{injected} \qquad (25)$$

$$\phi = \phi_{raw} - \delta iono_{injected} \qquad (26)$$

The error injected into the L2 measurements is computed by multiplying the L1 ionospheric error by $\alpha = f_1^2/f_2^2$, as the impact is frequency dependent. For the injected ionospheric error we consider a gradient consistent with the worst case of the German threat model [1] (specifically, a gradient slope of 140 mm/km and a maximum speed of 200 m/s). The gradient was injected at $t$ = 15 seconds and the ramp was stopped after 90 seconds, at t=105s, and was kept constant until t=250s, as illustrated in Figure 13. The error was injected on only one satellite, the satellite with the maximum $S_{apr,vert}$.

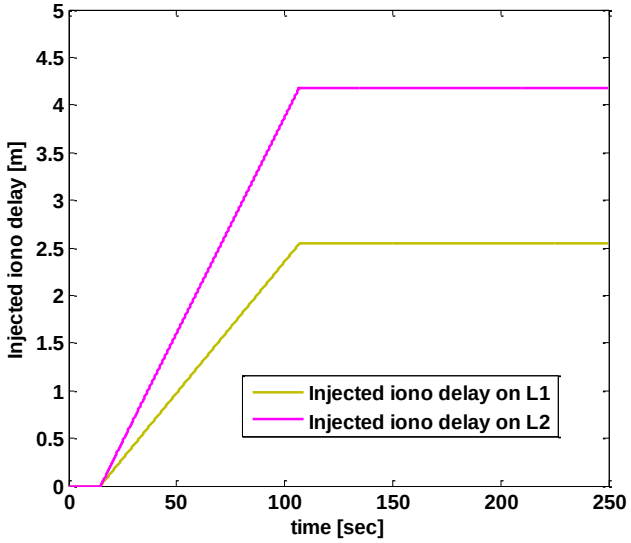


**Figure 13 Injected ionospheric errors on L1 and L2**

Figure 14 illustrates the effect of the injected ionospheric ramp as it propagates through the different smoothing filters.

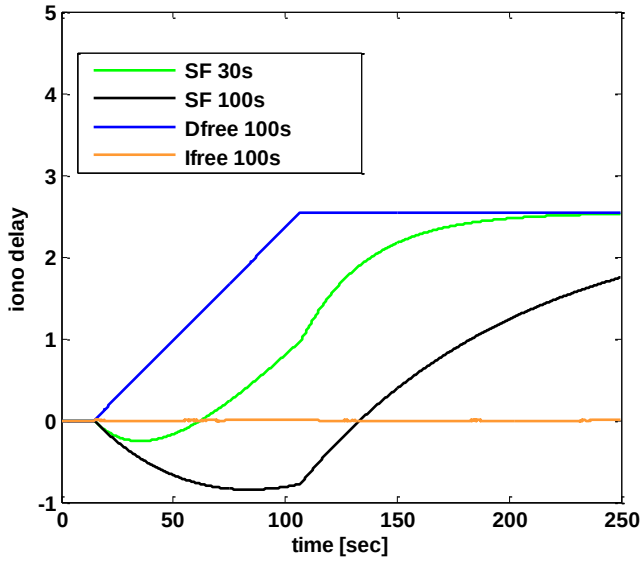


**Figure 14 Error in smoothed pseudoranges after injecting ionosphere error ramp**

**Single frequency 30 and 100-second smoothing (green and black curves):**

For single frequency smoothing, the resulting ionospheric error after the gradient is introduced at $t$ = 15 seconds first starts in negative direction because the impact of the gradient on carrier phase initially dominates the impact on code phase within the smoothing filter. After reaching a minimum that is a function of the smoothing time constant, the black and green curves in Figure 14 both start to increase into the positive direction as the impact on code phase takes over, with the 30-second smoothing filter reacting much faster than the 100-second filter.

Eventually, both filters converge to the maximum ionospheric error which was injected (recall that the injected gradient is stopped after 90 seconds, at t=105s). Again, the 30-second filter reaches this value much faster than the 100-second filter.

Airborne code carrier divergence (CCD) monitoring is part of the GAST-D architecture and is intended to detect satellites which are affected by large ionospheric temporal gradients. This monitor crossed its threshold and alerted the affected satellite 80 seconds after the onset of the gradient (i.e., at $t$ = 95 seconds). At this moment, the satellite was excluded from GAST-D solution. The output of the airborne CCD monitor together with its threshold of 0.0125 m/s is shown in Figure 15.

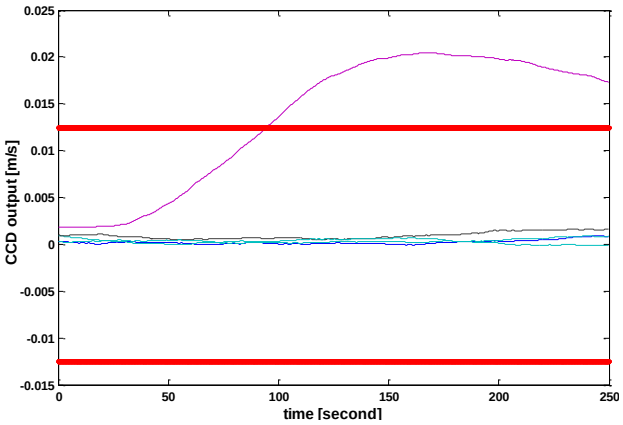


**Figure 15 CCD monitor output. The red curves mark the thresholds of the airborne CCD monitor (± 0.0125 m/s)**

**Dfree 100-second smoothing (blue curve):**

As shown previously in the section introducing the different smoothing techniques, the resulting error for the Dfree solution is exactly the ionospheric ramp injected into the measurements. The effect appears immediately without any delay and convergence time with the same sign as the injected error. The ramp in the Dfree output is not caused by code-carrier divergence but instead represents the actual ionospheric delay difference between the airborne receiver (where the ionospheric delay

increases as shown in Figure 13) and the ground receiver (where no increase in ionospheric delay is observed).

**Ifree 100-second smoothing (orange curve):**

As expected, the Ifree smoothing completely removes the effect of the injected ionospheric gradient.

Figure 16 shows the results of ionospheric gradients in the position domain. Vertical error is plotted under nominal conditions (subplot (a)) and after the injection the ionospheric error as shown in Figure 13 (subplot (b)).The resulting error behavior is consistent with the observation of the smoothing filter outputs.

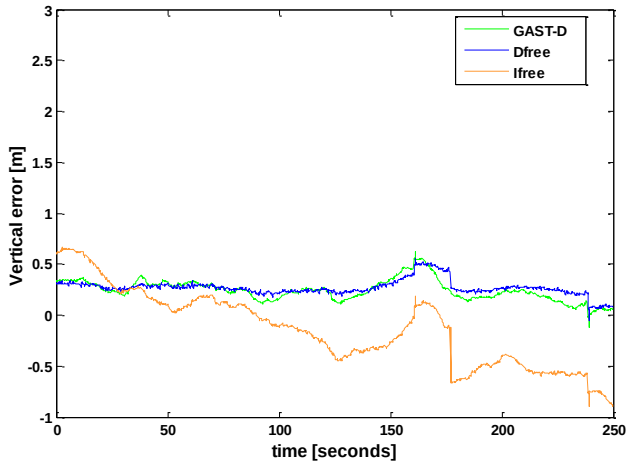


**(a)**

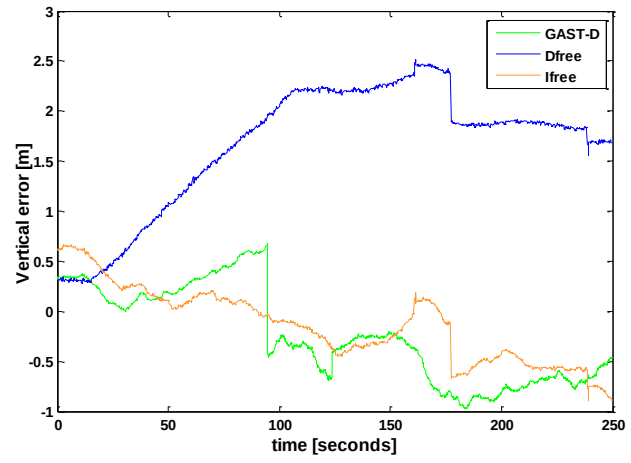


**(b)**

**Figure 16 Vertical error (a) under nominal conditions, and (b) after injecting the ionospheric error for SF GAST-D (green curve), Dfree (blue curve) and Ifree (orange curve)**

**Single frequency with 30-second smoothing (GAST-D output):**

In the single frequency GAST-D solution, the vertical error tends to go to zero due to the initial effect of carrier-phase dominance level and increases afterwards, as the effect smoothed pseudoranges comes to dominate and turns in the other direction. At $t$ = 95 seconds, the satellite is flagged by the CCD monitor and excluded from the GAST-D solution. The error jumps at this point, as the injected ionospheric error is no longer present in the calculated position.

**Dfree with 100-second smoothing:**

The vertical position error in the Dfree solution starts increasing due to the presence of the ionospheric error immediately once it is injected. After the ramp is stopped, the error remains approximately constant, as the differential ionospheric delay between airborne and ground remains at a constant value (in reality, the gradient would eventually arrive at the ground station and begin reducing the differential error). Note that, other than in the GAST-D scenario, no monitor to alert and exclude the affected satellite is used in the Dfree scenario. The effect of the ionospheric error can thus be seen in the position solution immediately and as long as the ramp is injected. However, Dfree in general provides improved detection capabilities for this kind of scenario which would allow for detection and exclusion faster than in GAST D.

**Ifree with 100-second smoothing:**

As the Ifree smoothed ranges are not affected by the injected ionospheric error, no impact is observed on the position solution. The jumps in vertical error at around $t$ = 175 seconds which are present in both nominal and anomalous scenarios and are due to a satellite geometry change (note that this change affects the Dfree solution as well).

## 7.0 CONCLUSION

We have presented an evaluation of single and multi-frequency GBAS performance under nominal and severe ionospheric gradient conditions. In the GBAS ground system, we examined the noise and multipath performance of signals on the newly available L5 frequency. Despite the fact that, on the raw measurements, noise and multipath errors were significantly lower on L5C compared to L1 C/A code, the assessment of $\sigma_{pr\_gnd}$ showed very similar results for all frequencies. This was attributed to the effect of code-carrier smoothing with a lengthy (100-second) time constant. In order to leverage the benefit of improved signal quality, a reduced smoothing time constant will be investigated in further studies.

Assessments of the airborne performance of the GAST-D and dual frequency algorithms were based on data collected during a flight trial which took place on 18 January 2013. No ionospheric anomalies were present during this flight, and the results matched expected behavior. Afterward, a severe ionospheric gradient was injected into raw measurements collected during the flight trial to assess the impact on single frequency and dual

frequency smoothing behavior. The results showed that single frequency and Dfree solutions have similar results under nominal conditions. Under the ionospheric gradient scenario, the Dfree solution reacts faster, and is consistent with the pattern of the injected gradient. The single frequency results contain ionospheric error from code carrier divergence due to the smoothing filter. They will react slower, depending on the smoothing time constant, and will converge later to the same maximum differential ionospheric error injected. Due to the realization of single frequency carrier smoothing, errors build up slower (and first in opposite direction) than in the Dfree case. The Ifree solution is much noisier and results in larger positioning errors compared to the other two techniques. Nominal performance is worse than with single frequency or Dfree smoothing and is also reflected in larger protection levels. It is, however, not affected by ionospheric disturbances.

## REFERENCES


[1] C. Mayer, B. Belabbas, N. Jakowski, M. Meurer, W. Dunkel, "Ionosphere Threat Space Model Assessment for GBAS", *Proceedings of ION International Technical Meeting, Savannah, GA, September 2009, pp. 1091-1099.*

[2] Eurocae ED-114A, "Minimum operational performance specification for global navigation satellite ground based augmentation system ground equipment to support category I operations", *France, 2013*

[3] H. Konno "Design of an aircraft landing system using dual-frequency GNSS," *Ph.D. thesis, December 2007*

[4] H. Konno, (2006) , " Evaluation of Two Types of Dual-Frequency Differential GPS Techniques under Anomalous Ionosphere Conditions"

[5] J. Lee, M. Luo, S. Pullen, Y.S. Park, P. Enge, M. Brenner , "Position-Domain Geometry Screening to Maximize LAAS Availability in the Presence of Ionosphere Anomalies", *Fort Worth, TX, September 2006, pp. 393-40*

[6] J. Lee, S. Pullen, S.d. Barua, and P. Enge, "Assessment of Nominal Ionosphere Spatial Decorrelation for LAAS", *Proceedings of IEEE/ION PLANS, San Diego, CA, April 2006, pp. 506-514.*

[7] L.H. Estey, C.M.Meertens, TEQC, "The multipurpose Toolkit for GPS/GLONASS Data", *GPS Solution, Vol. 3, No.1, 1999*

[8] M. Felux, et al, (2012), "Towards Full GAST-D Capability – Flight Testing using the DLR's Experimental GBAS Station", *Proceedings of ION International Technical Meeting, New Port Beach, CA, January 2012, pp. 1648-1654*

[9] McGraw A, T. Murphy, M. Brenner, S. Pullen, A.J. Dierendonck, "Development of the LAAS Accuracy Models", *Proceedings of ION International Technical Meeting, Salt Lake City, UT, September 2000, pp. 1212-1223.*

[10] Murphy et al. (2010), "Implications of 30-Second Smoothing for GBAS Approach Service Type D," *Proceedings of International Technical Meeting of The Institute of Navigation, San Diego, CA, January 2010, pp. 376-385.*

[11] P. Hwang, et al, "Enhanced Differential GPS Carrier-Smoothed Code Processing Using Dual-Frequency Measurements", *Navigation, J. of the Inst. of Navigation*, Vol. 46, No. 2., 1999

[12] R. Geiste, T. Kapol (2013), "Cockpit Visualization of Curved Approaches based on GBAS", *Navigation, J. of the Inst. of Navigation*, Vol. 60, No. 4, 2013

[13] RTCA DO-253C, "Minimum operational performance standards for GPS local area augmentation system airborne equipment*", Tech. Rep. DO-253C, RTCA, Washington, 2008*

[14] T. Dautermann, M. Felux, A. Grosh , " Approach service type D evaluation of the DLR GBAS testbed", GPS Solution, 2011, 2011, DOI 10.1007/s10291-011-0239-3